



Rate Constants of Electrochemical Reactions in a Lithium-Sulfur Cell Determined by Operando X-ray Absorption Spectroscopy

Dunyang Rita Wang,^{1,2} Deep B. Shah,^{2,3} Jacqueline A. Maslyn,^{2,3} Whitney S. Loo,³ Kevin H. Wujcik,^{2,3} Erik J. Nelson,⁴ Matthew J. Latimer,⁴ Jun Feng,⁵ David Prendergast,⁶ Tod A. Pascal,⁶ and Nitash P. Balsara^{2,3,7,*}

¹Department of Materials Science and Engineering, University of California, Berkeley, California 94720, USA

²Materials Sciences Division, Lawrence Berkeley National Laboratory, Berkeley, California 94720, USA

³Department of Chemical and Biomolecular Engineering, University of California, Berkeley, California 94720, USA

⁴Stanford Synchrotron Radiation Lightsource, SLAC National Accelerator Laboratory, Menlo Park, California 94025, USA

⁵Advanced Light Source, Lawrence Berkeley National Laboratory, Berkeley, California 94720, USA

⁶Molecular Foundry, Lawrence Berkeley National Laboratory, Berkeley, California 94720, USA

⁷Energy Technologies Area, Lawrence Berkeley National Laboratory, Berkeley, California 94720, USA

The reduction of sulfur during discharge in a lithium-sulfur (Li-S) cell is known to occur in a series of reaction steps that involve lithium polysulfide intermediates. We present an operando study of the discharge of a solid-state Li-S cell using X-ray absorption spectroscopy (XAS). In theory, the average chain length of the polysulfides, $x_{\text{avg,cell}}$, at a given depth of discharge is determined by the number of electrons delivered to the sulfur cathode. The dependence of $x_{\text{avg,cell}}$ measured by XAS on the depth of discharge is in excellent agreement with theoretical predictions. XAS is also used to track the formation of Li_2S , the final discharge product, as a function of depth of discharge. The XAS measurements were used to estimate rate constants of a series of simple reactions commonly accepted in literature.

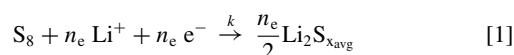
© The Author(s) 2018. Published by ECS. This is an open access article distributed under the terms of the Creative Commons Attribution 4.0 License (CC BY, <http://creativecommons.org/licenses/by/4.0/>), which permits unrestricted reuse of the work in any medium, provided the original work is properly cited. [DOI: 10.1149/2.0981814jes]



Manuscript submitted August 17, 2018; revised manuscript received October 5, 2018. Published November 9, 2018.

Lithium-sulfur (Li-S) batteries have been considered as attractive alternative to current Li-ion batteries due to their large theoretical capacity (1672 mAh/g) and theoretical energy density (2600 Wh/kg). Sulfur is a particularly attractive cathode material for large format cells because it is cheap and abundant.¹⁻⁴ While there are numerous practical problems that have prevented the commercialization of rechargeable Li-S batteries, a significant barrier is the lack of understanding of the reaction mechanism that underlies this chemistry.⁵⁻¹⁰ The redox reactions in the sulfur cathode occur in steps.¹¹ Some of the products in these steps are soluble lithium polysulfides intermediates.¹²⁻¹⁴ The chemical formulae of lithium polysulfides are generally expressed as Li_2S_x where x , the length of the sulfur chain in the polysulfide is generally assumed to be between 2 and 8.¹⁵ The dissolution of these species into the electrolyte is one of the primary problems that must be overcome before rechargeable Li-S batteries are commercialized. It also interferes with fundamental studies of redox reactions in the sulfur cathode.

The discharge reaction in the sulfur cathode of a Li-S cell can be written as Equation 1.

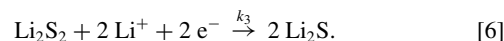
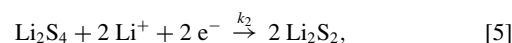
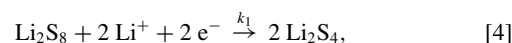
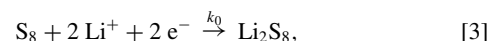


We define n_e as the moles of electrons delivered to the sulfur cathode per mole of S_8 in the cathode. The discharge reaction is complete when $n_e = 16$ and the only product in the cathode is Li_2S . Our interest is to determine the state of the cathode during the intermediate steps of the discharge process. It is well known that numerous partially reduced sulfur species exist in the cathode during these intermediate steps. Despite these complexities, Equation 1 must hold. In other words, the distribution of polysulfides obtained at a particular value of n_e must be such that the average chain length of the polysulfides, x_{avg} , is given by Equation 2, which arises due to mole balance of sulfur in Equation 1.

$$x_{\text{avg}} = \frac{16}{n_e} \quad [2]$$

To our knowledge, the validity of Equation 2 has not been experimentally established.

Many reactions have been proposed¹¹ for the stepwise reduction of sulfur. We begin our discussion with a simple series of steps given below:



In the simplest case, the overall sulfur reduction reaction rate is governed by the discharge rate imposed on the Li-S cell. This will be true if effects such as transport limitations in the electrolyte and blocking of electrode surfaces due to insulating products are negligible. The discharge rate is typically expressed as C/τ where τ is the number of hours required to fully discharge the cathode. The overall rate of the discharge reaction is controlled by dn_e/dt , which is held constant during a galvanostatic discharge. If we start with a sulfur cathode containing m grams of sulfur (0.171 mg), and discharge it with a current, i in mA (0.0143 mA), then n_e at a given time, t in hours, is given by Equation 7.

$$n_e = \frac{16it}{1672m} \quad [7]$$

where we have used the fact that the theoretical capacity of the sulfur cathode is 1672 mAh per g of sulfur.

The electrons delivered by the potentiostat to the cathode participate in all of the Reactions 3–6. The distribution of polysulfides in the cathode at time t will be determined by the relative rate constants, k_0/k_1 , k_2/k_1 , and k_3/k_1 ; see Reactions 3–6 for definitions of k_i . Our use of k_1 to normalize rate constants will be made clear shortly. Our objective is to estimate some of the relative rate constants that characterize reactions in a model sulfur cathode.

*Electrochemical Society Member.

⁷E-mail: nbalsara@berkeley.edu

In the past decade, different techniques have been used to study the reaction mechanism in Li-S cells. Each technique has its own advantages and limitations.^{9,11} Electrochemical measurements such as cyclic voltammetry (CV)^{16,17} and rotating-ring disk electrode (RRDE)¹⁸ are powerful approaches for determining the state of discharge but lack of the ability to distinguish different reaction products. X-ray diffraction (XRD) can be used to detect the presence of crystalline species such as Li_2S and S_8 but it is insensitive to the presence of amorphous polysulfides.^{19,20} Uv-vis,^{21–23} Raman,^{24,25} NMR^{26,27} and X-ray absorption spectroscopy (XAS)^{28–39} can, in principal be used to detect polysulfides. In References 20–38, measured spectra are used to infer the presence of certain specific polysulfide species. Such inferences rely on spectral signatures of pure polysulfides. Unfortunately there is no consensus on how polysulfides might be purified nor is there consensus on unique spectral fingerprints of different polysulfides.

In this paper, we present results of an operando XAS study of a solid-state Li-S cell. Our measurements enable independent measurements of x_{avg} and n_e , thereby enabling a test of the validity of Equation 2. The XAS data also enable determination of the moles of Li_2S formed during discharge. These measurements enable determination of relative rate constants that characterize sulfur oxidation in the cathode, k_2/k_1 and k_3/k_1 .

Experimental

The separator/electrolyte and cathode were stored inside an argon-filled glove box (MBraun) with H_2O and O_2 concentrations maintained at less than 0.1 ppm. Cell assembly was performed inside the same glove box.

Separator/electrolyte film preparation.—The separator/electrolyte films were prepared using a block copolymer of polystyrene-*b*-poly(ethylene oxide) (SEO) synthesized using methods described in the work by Hadjichristidis et al.⁴⁰ and purified using methods described in the work by Teran et al.⁴¹ The molecular weights of polystyrene and poly(ethylene oxide) are 200 kg/mol and 222 kg/mol, respectively. Lithium perchlorate (LiClO_4 , Sigma-Aldrich) was dried for 24 hours under vacuum at 90°C before use. The separator/electrolyte films containing SEO and LiClO_4 were prepared according to the method described in the work by Wujcik et al.⁴² The thickness of separator/electrolyte film used was 22 μm .

Cathode preparation.—Cathode slurries containing S_8 (Alfa Aesar), Li_2S (Sigma-Aldrich) carbon black (Denka), LiClO_4 , and SEO (identical LiClO_4 /SEO composition to that of the electrolyte separator) was mixed in *n*-methylpyrrolidone (NMP). The slurry was composed of 89 wt% of NMP. S_8 and Li_2S were mixed in a 256:46 weight ratio to produce Li_2S_x with an average x value of 8 as the starting material. Due to the insulating properties, both ionic and electronic, of S_8 , Li_2S_8 was used as the starting material. Since Li_2S_8 is soluble in the slurry, we expect a uniform distribution of the sulfur-containing species in the cathode (as opposed to insoluble S_8), and we posit that this leads to better contact between the active material, the electrolyte and carbon black in the dry cathode. The slurry was mixed overnight at 90°C and subsequently mixed using a homogenizer (Polytron) set to 15,000 RPM. Homogenization was done for five minutes and repeated three times, with two minute rests between each cycle to prevent the solution from heating up to undesirable temperatures. The resulting slurry was then casted onto an 18 μm thick aluminum foil current collector using a doctor blade. The film was dried under Argon at 60°C for 10 hours and then placed under static vacuum overnight at room temperature. The resulting cathode had an average thickness of 16 μm , with the resulting composition: 12.8 wt% Li_2S_8 , 51.4 wt% SEO, 5.5 wt% LiClO_4 , and 30.3 wt% carbon. Our use of a relatively thin sulfur cathode with low sulfur loading

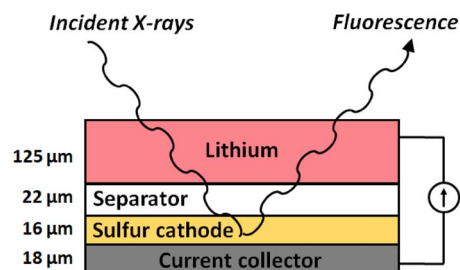


Figure 1. Schematic of a Li-S cell used for operando XAS study.

was motivated by our desire to minimize self-absorption in the XAS experiments.

Cell assembly and cycling.—A pouch cell was prepared according to the method described in the work by Wujcik et al.³⁷ The electrolyte film was placed on the cathode. The lithium metal anode was then placed over the electrolyte film. The cathode-electrolyte-anode stack was tabbed and sealed in a pouch cell was kept at rest at room temperature in an argon environment for 48 hours before taking measurements. The cell was then taken out of the argon-filled glove box and placed on a sample holder connected to a heating source. It was then held at a temperature of 90°C for 1.5 hours to ensure good electrical contact between the cathode, electrolyte, and anode layers. The cell was then charged to partially form S_8 , and then discharged at 90°C at a C/20 rate using a VMP3 Potentiostat (Bio-Logic). High temperature operation is necessary due to the limited conductivity of polymer electrolytes at low temperatures.⁴³ Figure 1 shows a schematic of the assembled cell. The discharge and charge rate was calculated using the measured mass of the cathode electrode, the known weight percent of sulfur in the cathode, and assuming a theoretical capacity of 1672 mA-h/g for sulfur. The voltage window was kept between 1.5 V and 3.0 V.

X-ray absorption spectroscopy.—XAS measurements were performed at beamline 4–3 of the Stanford Synchrotron Radiation Light-source. Preliminary XAS experiments were performed at beamline 5.3.1 of the Advanced Light Source. Measurements were taken in fluorescence mode using a four element Vortex detector, with 0.1 eV energy resolution around the absorption K-edge. One scan took roughly 10 minutes to collect, equivalent to roughly 13.9 mA-h/g of capacity passed per scan. The beam spot size was 2 mm² and was not moved during cycling. The cell holder was inside a helium-filled chamber during the in operando measurements. Calibration of the X-ray energy was performed using sodium thiosulfate (Sigma-Aldrich), setting the first peak maximum to 2472.02 eV.

XAS spectra analysis.—All spectra were analyzed using the Athena X-ray absorption spectroscopy program. Raw XAS spectra were used to calculate the “total sulfur” intensity based on methods described by our previous work.⁴² For peak deconvolution and product analysis, all spectra were normalized and self-absorption corrected using the Athena XAS analysis package. The initial spectra were fit with 4 Gaussian peaks and a step function. After 50 mA-h/g the spectra were fitted with 6 Gaussians to account for the increasing skewness in the main-edge peak due to blueshift of the main-edge peak for mid-chain and short-chain polysulfides. Example of fitting an experimental spectra with 6 Gaussian peaks and a step function is shown in Figure S1.

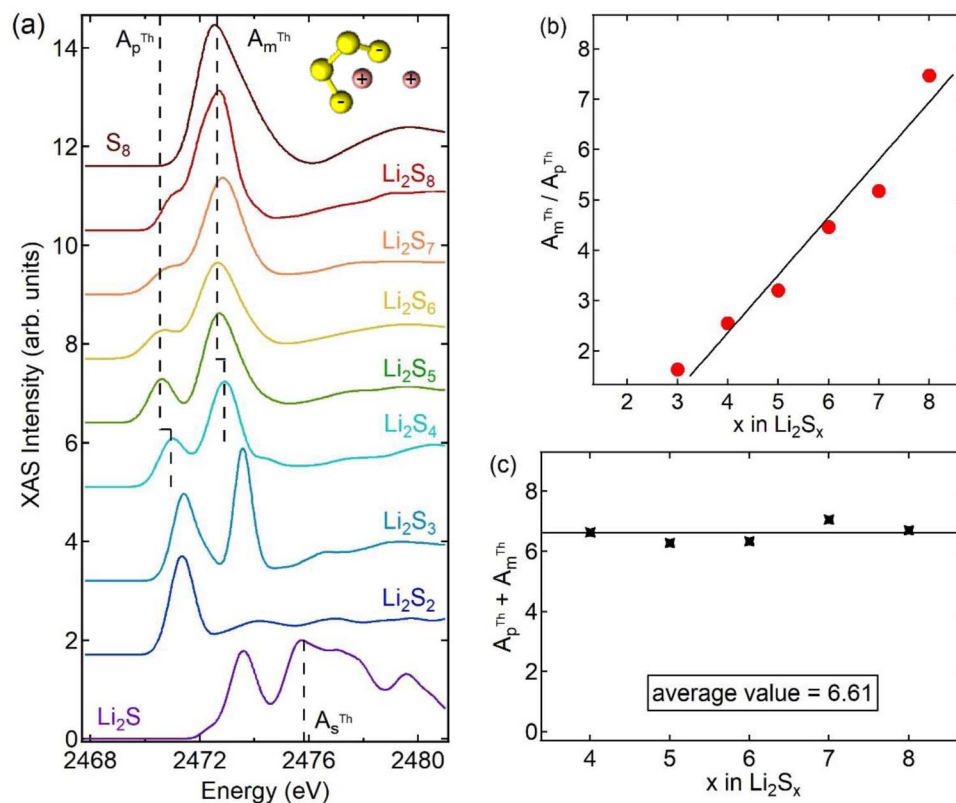


Figure 2. (a) Theoretical XAS spectra from Pascal et al.,⁴⁴ (b) linear relationship between x for Li_2S_x ($3 \leq x \leq 8$) and the area ratio of main-edge peak to pre-edge peak, A_m/A_p , and (c) sum of pre-edge and main-edge peak areas per mole of Li_2S_x ($4 \leq x \leq 8$) from theoretical spectra.

Results and Discussion

Theoretical XAS spectra analysis.—Theoretical XAS spectra for different lithium polysulfides were presented by Pascal et al. in a previous publication,⁴⁴ and the results are summarized in Figure 2a. In the inset of Figure 2a, we show a typical molecular conformation of one of the polysulfides, Li_2S_8 . Polysulfides with chain length between 3 and 8 have two charged terminal sulfurs and the remainder of the internal sulfurs are uncharged. The two kinds of sulfurs give rise to two distinctive XAS features: a pre-edge peak corresponding to the two charged end-chain sulfurs and a main-edge peak corresponding to the internal sulfurs. The area under the theoretical pre-edge peak of each polysulfide is denoted by A_p^{Th} . Similarly the area under the theoretical main-edge peak of each polysulfide is denoted by A_m^{Th} . The spectral features of the polysulfides are approximated as a sum of Gaussian peaks and the areas under selected peaks were used to compute A_p^{Th} and A_m^{Th} as outlined in Figure S2. In Figure 2b we plot the ratio, $A_m^{\text{Th}}/A_p^{\text{Th}}$, as a function of polysulfide chain length, x in Li_2S_x ($3 \leq x \leq 8$). The line in Figure 2b is a least squares linear fit. We use this linear fit as a “calibration” to determine the average chain length of polysulfides in our cell, x_{avg} , using measured values of pre-edge and main-edge areas, A_p and A_m . The straight line in Figure 2b can be represented as

$$x = 0.8732A_m/A_p + 1.9326. \quad [8]$$

In Figure 2c we plot the sum, $(A_p^{\text{Th}} + A_m^{\text{Th}})$, as a function of x in Li_2S_x ($4 \leq x \leq 8$). To a good approximation, $(A_p^{\text{Th}} + A_m^{\text{Th}})$ is 6.61, independent of x . The theoretical spectrum of Li_2S contains a unique peak at 2476 eV that is not present in any of the polysulfides. The area under this peak, A_s^{Th} , was calculated by approximating the theoretical Li_2S spectrum by a sum of Gaussian peaks as shown in Figure S3. The value of A_s^{Th} is 3.07.

Thus,

$$\frac{A_s^{\text{Th}}}{A_p^{\text{Th}} + A_m^{\text{Th}}} = \frac{3.07}{6.61} = 0.46. \quad [9]$$

We use this to estimate the moles of Li_2S in our cell is determined by estimating the area under the peak at 2476 eV, A_s .

Total sulfur signal.—The XAS cell was made with Li_2S_8 in the cathode. Our use of Li_2S_8 facilitated dispersion of the sulfur species in the cathode. Our main objective is to determine the state of the sulfur-containing cathode as the cell is discharged. We used a relatively thin cathode and adjusted the sulfur content in the cathode to ensure that all of the sulfur-containing species in the cell could be detected by XAS. The cell was prepared 48 hours before the XAS experiment, stored at room temperature in an argon glove box, placed in the XAS sample stage, heated to 90°C for 1.5 h, charged at C/20 until the voltage reached 3.0 V, and then discharged at C/20. Figure 3a shows all of the raw XAS spectra during these experiments. The magnitude of the high energy plateau attained between 2500 and 2575 eV is indicative of the total amount of sulfur detected. We define I_0 to be the average value of the raw XAS signal between 2500 and 2575 eV obtained just prior to discharge. We define I_n as the average value of the raw XAS signal in the same energy range obtained during other scans. The time dependence of the cell potential during these experiments is shown in Figure 3b. The corresponding values of I_n/I_0 versus time shows are shown in Figure 3c.

If our cell was perfectly designed, then I_n/I_0 would be independent of time. In our case, I_n/I_0 increased by about 12% during the heating step, and increased by about another 16% during the charging step. This is attributed to the dissolution of Li_2S_8 into the separator during the heating and charging steps. Because the anode side faces the incoming X-ray source, the incident intensity on the sulfur-containing species in the separator is higher than that on the sulfur-containing

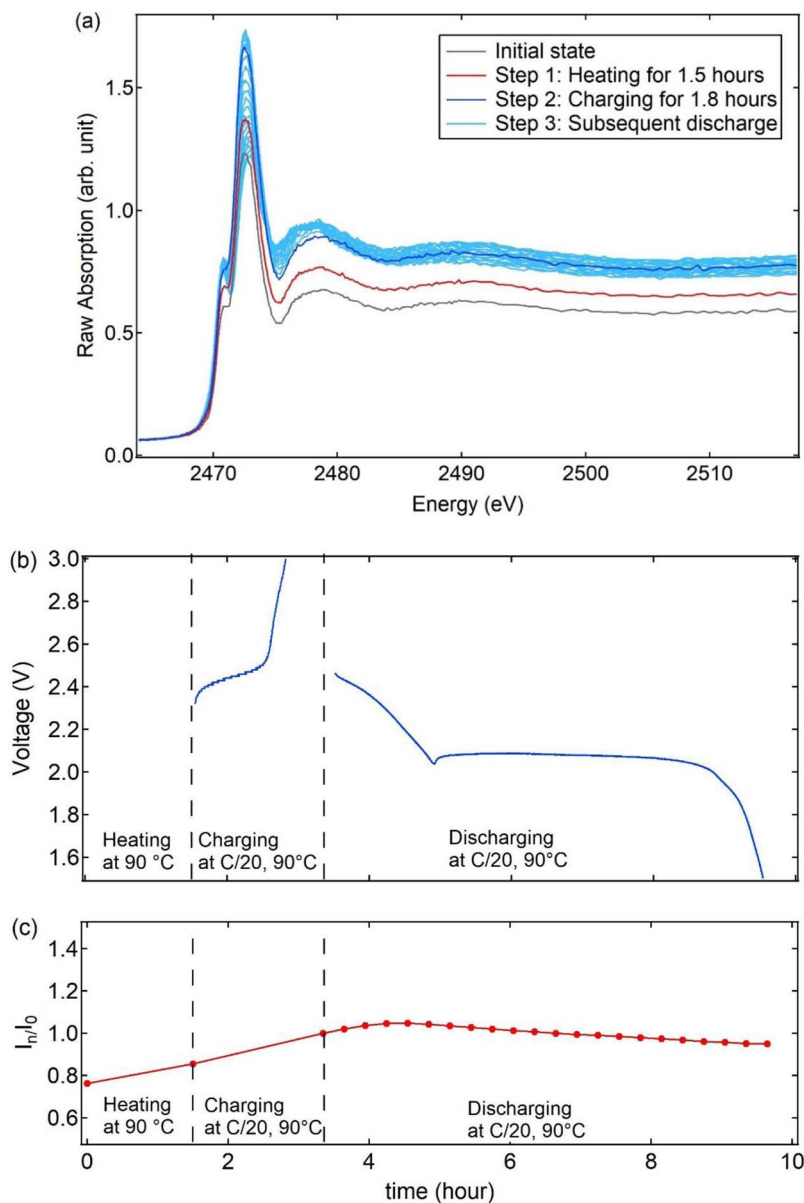


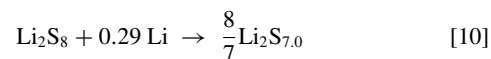
Figure 3. (a) All raw XAS spectra, (b) time dependence of voltage and (c) time dependence of I_n/I_0 before and during cycling.

species in the cathode. Similarly, the fluorescence signal from the sulfur-containing species in the separator is more efficiently detected because the anode side also faces the detector. Thus, the diffusion of sulfur-containing species into the separator is expected to increase I_n/I_0 . During the discharge step, however, I_n/I_0 remained approximately constant, varying between 1.05 and 0.95. The constancy of I_n/I_0 during discharge indicates that all (or nearly all) of the products of sulfur reduction were detected by XAS experiment. We therefore conclude that there is no further change in the concentration of polysulfides in the separator during the discharge step.

Discharge products from spectra.—The raw spectra shown in Figure 3a were normalized and corrected for self-absorption. All of the normalized spectra exhibited a pre-edge peak around 2471 eV and a main-edge peak around 2473 eV. This enables calculation of the areas under the pre-edge, A_p , and main-edge peak, A_m . These areas can be used to determine the average polysulfide chain length in the cell, $x_{\text{avg,cell}}$ (x for Li_2S_x), using Equation 8. After the heating step, $x_{\text{avg,cell}}$ equals 7.0. After the charging step, $x_{\text{avg,cell}}$ reached 8.1.

An ideal cell would be one wherein all of the Li_2S_8 remained in the cathode during storage prior to the XAS experiment and during

the heating step. In other words, $x_{\text{avg,cell}}$ would equal 8.0 in the ideal cell after the heating step. It is evident that our cell is not ideal as $x_{\text{avg,cell}}$ is 7.0 at the end of the heating step. This departure from ideality is attributed to the dissolution of Li_2S_8 into the separator, subsequent reactions with the lithium metal anode, and shuttling of the resulting shorter polysulfides back into the cathode. We posit that during storage and the heating step, 0.29 moles of Li from the anode per mole of Li_2S_8 is consumed to reduce the average chain length from 8 to 7.0, as indicated in Equation 10.



The cell with $x_{\text{avg,cell}} = 7.0$ was then charged at a C/20 rate. In an ideal cell, all of the sulfur-containing species would be converted to S_8 after charging. If this were true, $x_{\text{avg,cell}}$ would equal infinity after the charging step. Instead we find that the average chain length increased from 7.0 to 8.1 during the charging step. During the charging step, 1.02 moles of electrons were delivered to the anode per mole of S_8 in the cell ($t = 1.27$ h in Equation 7). If all of these electrons participated in the oxidation of $\text{Li}_2\text{S}_{7.0}$, then $x_{\text{avg,cell}}$ at the end of charging step would have been 14.2. The observed departure from ideality during the charging step is attributed to the reduction of polysulfide species at

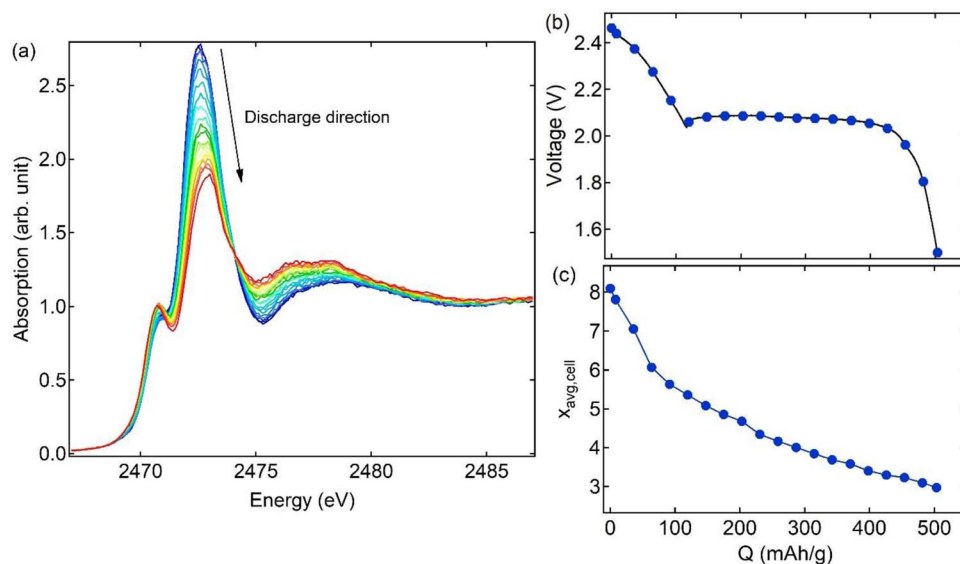


Figure 4. (a) Normalized and self-absorption corrected in operando XAS spectra and (b) voltage profile and average polysulfide chain length during discharge.

the anode/separators interface instead of complete conversion into Li metal. We conclude that these side reactions consume 0.73 moles of electrons per mole of S_8 . The remainder participated in the oxidation of $Li_2S_{7.0}$ and the concomitant reduction of Li^+ to Li metal:

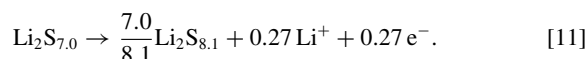


Figure 4a shows the self-absorption-corrected normalized spectra during discharge. Figure 4b shows the dependence of cell potential versus capacity, Q , during discharge. The XAS spectra in Figure 4a contain standard signatures of polysulfides: a main-edge peak with area A_m and a pre-edge peak with area A_p . Using methods described above and Equation 8 we determined $x_{avg,cell}$ as a function of capacity, and the results are shown in Figure 4c. (The spectra do not contain signatures of polysulfide radicals that are sometimes observed in Li-S cells.^{34,37,45}) The relatively low discharge capacity, 503 mAh/g, of our cell is due to non-idealities discussed above. During discharge, $x_{avg,cell}$ decreased monotonically from 8.1 to 3.0. In the early stage of discharge, $Q < 100$ mAh/g, $x_{avg,cell}$ decreases rapidly with increasing Q . In the late stage of discharge, $Q > 100$ mAh/g, $x_{avg,cell}$ decreases slowly with increasing Q .

The measured XAS spectrum at the end of discharge is shown in Figure 5a. In addition to the pre-edge and main-edge peaks at 2471 eV and 2473 eV, an additional peak is observed at 2476 eV. The three dashed lines in Figure 5a correspond to the characteristic energies of these peaks. As discussed above, the theoretical spectra in Figure 2a show that the peak at 2476 eV is a unique signature of Li_2S and it

arises due to the crystalline nature of this compound.⁴⁴ In addition to determining A_p and A_m , we also determined A_s for each of the spectra shown in Figure 4a. We define m_{Li_2S} as the moles of Li_2S formed per mole of polysulfides. In theory, m_{Li_2S} is given by

$$m_{Li_2S} = \frac{1}{0.46} \left(\frac{A_s}{A_p + A_m} \right) \quad [12]$$

Where the constant 0.46 is based on analysis of the theoretical spectra and Equation 7. Note that in this analysis, Li_2S is not considered as a polysulfide. In Figure 5b, we plot $\frac{A_s}{A_p + A_m}$ on the left axis and m_{Li_2S} , on the right axis versus Q . The moles of Li_2S formed is low in the early stage of discharge, $Q < 100$ mAh/g, but increases rapidly in the late stage of discharge, $Q > 100$ mAh/g. Whether or not Li_2S forms in the early stage of discharge remains an interesting, open question. We suspect that the values we have obtained are due to limitations of our spectral fitting procedure. In our cell, m_{Li_2S} remains small reaching a maximum value of 0.24 at the end of discharge. Note that the theoretical spectrum of Li_2S contains a feature at 2474 eV. In principal, we should correct the measured values of A_m to account for the fact that some of the signal at the main-edge peak is due to Li_2S . This correction is small because m_{Li_2S} remains small in our experiment.

Relating average discharge products to n_e .—The dependence of $x_{avg,cell}$ on n_e during discharge is shown in the inset in Figure 6. We have assumed that all of the electrons delivered to the cathode are

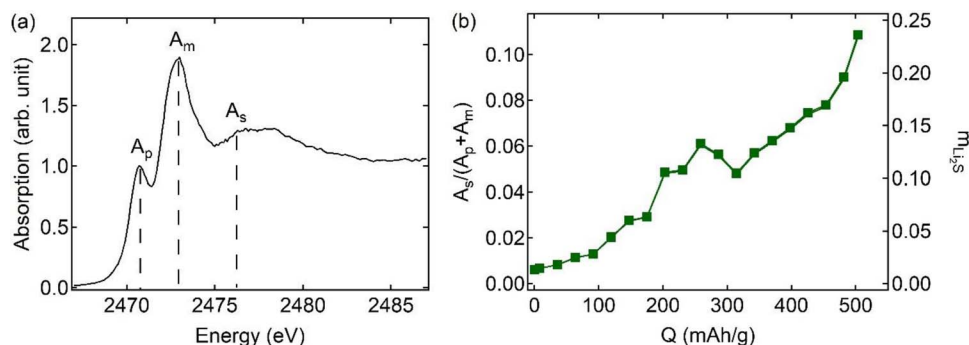


Figure 5. (a) Illustration of peaks with areas A_p , A_m , and A_s for a discharged spectrum, and (b) ratio of 2476 eV peak, A_s , to sum of peak areas for pre-edge and main-edge, $A_p + A_m$, on the left axis and moles of Li_2S formed per mole of polysulfides, m_{Li_2S} , on the right axis versus discharge capacity.

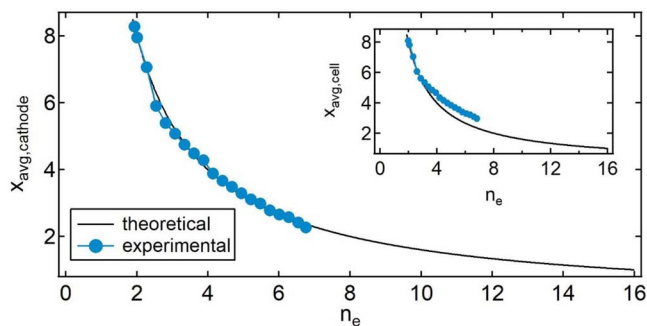


Figure 6. Theoretical and experimental average chain length of sulfur-containing species in the cathode, $x_{\text{avg,cathode}}$ and in the cell $x_{\text{avg,cell}}$, vs number of electrons delivered per S_8 molecule, n_e .

consumed by the Li_2S_8 molecules; side-reactions such as the formation of the solid electrolyte interphase (SEI) are ignored. The curve in the inset represents the theoretical prediction, Equation 2. The theoretical value of n_e corresponds to a cathode that contains pure S_8 at the beginning of discharge (see Equation 1). In the experiments however, our cathode to a good approximation contains Li_2S_8 at the beginning of discharge. The data points in the inset in Figure 6 represent experimental values of $x_{\text{avg,cell}}$ and n_e . $x_{\text{avg,cell}}$ was obtained from measurements of A_p and A_m using Equation 8. To account for the fact that the discharge begins with Li_2S_8 , we set n_e to a value close to 2 at the beginning of discharge and it is incremented based on Equation 7. The actual value used was 1.97 to obtain a perfect match between the experimental data and the theoretical prediction at the beginning of discharge. It is evident that the decrease in the average chain length of sulfur-containing species in the cell is in reasonable agreement with Equation 2.

Our analysis above indicates that some of the Li_2S_8 molecules located in the cathode when the cell was made diffuses into the separator and reacted with Li metal. This results in an average composition of $\text{Li}_2\text{S}_{7.0}$ before charging. The polysulfides in the separator not in contact with electronically conducting materials cannot participate in charge or discharge reactions. Their presence also affects our ability to detect the nature of the sulfur-containing species inside the cathode. We posit that these effects are responsible for the deviations between theory and experiment in the inset of Figure 6. We define $x_{\text{avg,cathode}}$ as the average length of sulfur-containing species in the cathode. We assume that the average length of the sulfur-containing species in the separator is fixed at 7.0 during the discharge process. Our cell thus contains two layers with different concentrations of sulfur. Given the agreement seen in the inset of Figure 6, we conclude that most of the sulfur is in the cathode. Specifically, in our model, we assumed that 90% of the sulfur atoms are in the cathode and 10% of the sulfur atoms are in the separator. This enables calculations of the transmission coefficients of the two layers of our cell based on the known absorption coefficients of sulfur and the other elements in our cell. These calculations indicate that the transmission coefficient of the separator layer, $T_{\text{sep}} = 0.623$, while that of the cathode layer, $T_{\text{cathode}} = 0.398$. The distance between the two layers is set to 19 μm based on the geometry of our cell. (We assume for simplicity that all of the sulfur-containing species are located in the middle of each layer.) The measured value of $x_{\text{avg,cell}}$ reflects the length of sulfur-containing species in both the cathode and separator ($x_{\text{avg,cathode}}$, $x_{\text{avg,sep}}$) with a weighting function that depends on the sulfur content and the transmission coefficient of each layer. This is quantified by Equation 13.

$$x_{\text{avg,cathode}} D_{\text{cathode}} + x_{\text{avg,sep}} D_{\text{sep}} = x_{\text{avg, cell}} \quad [13]$$

where D_{cathode} and D_{sep} reflect the weighting functions as shown in Equations 14 and 15.

$$D_{\text{cathode}} = \frac{0.9 T_{\text{cathode}}}{0.9 T_{\text{cathode}} + 0.1 T_{\text{sep}}} = 0.852 \quad [14]$$

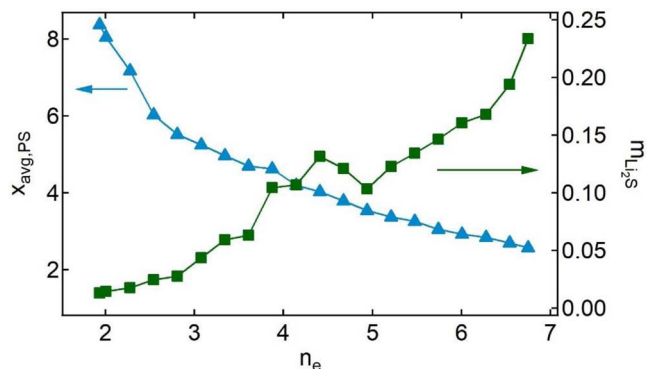


Figure 7. Average polysulfide chain length inside the cathode, $x_{\text{avg,PS}}$, on the left axis, and molar ratio of Li_2S to polysulfides, $m_{\text{Li}_2\text{S}}$, vs number of electrons delivered per S_8 molecule, n_e .

$$D_{\text{sep}} = \frac{0.1 T_{\text{sep}}}{0.9 T_{\text{cathode}} + 0.1 T_{\text{sep}}} = 0.148 \quad [15]$$

Since $x_{\text{avg,sep}} = 7.0$, we can calculate $x_{\text{avg,cathode}}$ corresponding to each value of $x_{\text{avg,cell}}$. Figure 6 shows the dependence of $x_{\text{avg,cathode}}$ versus n_e . The agreement between theory and experiment reflects the fact that the data are consistent with our assumption that 10% of the sulfur atoms are lost in the separator and hence not available for redox reductions. Our analysis indicates that $x_{\text{avg,cathode}}$ at the start of discharge is 8.28 while $x_{\text{avg,cathode}}$ at the end of discharge is 2.28 (see Figure 6).

The XAS peak at 2476 eV enables detection of Li_2S . It is therefore helpful to distinguish between Li_2S and other sulfur-containing species, namely polysulfides (Li_2S_x , $2 \leq x \leq 8$). We define $x_{\text{avg,PS}}$ as the average length of polysulfides. We calculate $x_{\text{avg,PS}}$ using the following equation:

$$x_{\text{avg,PS}} = (1 + m_{\text{Li}_2\text{S}}) x_{\text{avg,cathode}} - m_{\text{Li}_2\text{S}} \quad [16]$$

We arrive at this equation based on the sulfur mole balance in the cathode. For each mole of polysulfides ($\text{Li}_2\text{S}_{x_{\text{avg,PS}}}$) in the cathode we have $m_{\text{Li}_2\text{S}}$ moles of Li_2S , and together these compounds gives $(1 + m_{\text{Li}_2\text{S}})$ moles of $\text{Li}_2\text{S}_{x_{\text{avg,cathode}}}$.

The final result of our analysis of the XAS data is given in Figure 7 where $x_{\text{avg,PS}}$ and $m_{\text{Li}_2\text{S}}$ are plotted as a function of n_e .

It is not possible to identify a particular pathway that is consistent with the data in Figure 7. We used the principle of parsimony to interpret these data. In particular we used a model presented in the introduction beginning with Equation 4 and ending with Equation 6. We define C_8 , C_4 , C_2 , C_1 to be the molar concentrations of Li_2S_8 , Li_2S_4 , Li_2S_2 , and Li_2S , respectively, and assume that the reactions are limited by the concentrations of the sulfur-containing species. We expect this to be true at extremely low C rates. The simplest rate expressions for Reactions 4 through 6 are given below:

$$\frac{dC_8}{dt} = -k_1 C_8, \quad [17]$$

$$\frac{dC_4}{dt} = 2 k_1 C_8 - k_2 C_4, \quad [18]$$

$$\frac{dC_2}{dt} = 2 k_2 C_4 - k_3 C_2, \quad [19]$$

$$\frac{dC_1}{dt} = 2 k_3 C_2. \quad [20]$$

Since electrons are consumed in all three reactions,

$$\frac{dn_e}{dt} = -2 (k_1 C_8 + k_2 C_4 + k_3 C_2). \quad [21]$$

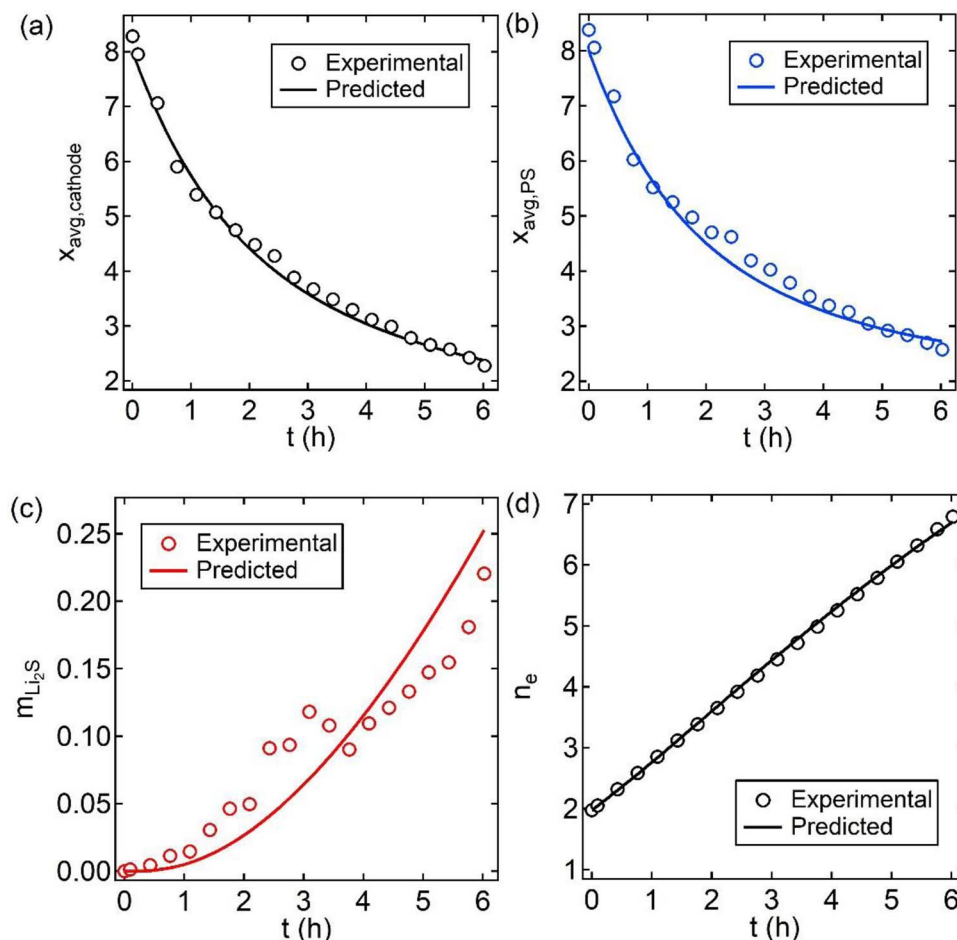


Figure 8. Comparing experimental measures and the predicted values of (a) $x_{\text{avg,cathode}}$, (b) $x_{\text{avg,PS}}$, (c) $m_{\text{Li}_2\text{S}}$, and (d) n_e versus t , time in hours, using the three-reaction model fitted with $k_1 = 0.368 \text{ h}^{-1}$, $k_2 = 3/4 k_1$, and $k_3 = 1/6 k_1$.

The measured quantities, $x_{\text{avg,cathode}}$, $x_{\text{avg,PS}}$, and $m_{\text{Li}_2\text{S}}$, are related to the molar concentrations of the sulfur-containing species:

$$x_{\text{avg,cathode}} = \frac{8 C_8 + 4 C_4 + 2 C_2 + C_1}{C_8 + C_4 + C_2 + C_1}, \quad [22]$$

$$x_{\text{avg,PS}} = \frac{8 C_8 + 4 C_4 + 2 C_2}{C_8 + C_4 + C_2}, \quad [23]$$

$$m_{\text{Li}_2\text{S}} = \frac{C_1}{C_8 + C_4 + C_2}. \quad [24]$$

Equations 17 through 24 were integrated numerically for specific values of k_1 , k_2 , and k_3 , with initial conditions $C_8 = 1$, $C_4 = C_2 = C_1 = 0$. The solved C_8 , C_4 , C_2 , C_1 at each t are used to predict $x_{\text{avg,cathode}}$, $x_{\text{avg,PS}}$, $m_{\text{Li}_2\text{S}}$, and n_e at each t . The symbols in Figure 8 show the experimentally determined values of $x_{\text{avg,cathode}}$, $x_{\text{avg,PS}}$, $m_{\text{Li}_2\text{S}}$, and n_e , respectively, as a function of time, t . The experimental values of $m_{\text{Li}_2\text{S}}$ in Figure 8c were subtracted by a constant so that $m_{\text{Li}_2\text{S}}$ at $t = 0$ is zero. This subtraction is necessary as the spectral signal at any given energy is not identically zero even if the species is absent due to factors such as contributions from neighboring excitations and background subtraction inaccuracies. The curves in Figure 8 show results of the numerical integration for $k_1 = 0.368 \text{ h}^{-1}$, $k_2 = 3/4 k_1$, and $k_3 = 1/6 k_1$. It is evident that the measurements are consistent with the proposed model. Our analysis indicates that the rate of reduction of sulfur-containing species decreases with decreasing chain length. To our knowledge, these are the first estimates of reaction rate constants for discharge reactions in the cathode of a Li-S cell.

Figure 9 plots the predicted concentrations of Li_2S_8 , Li_2S_4 , Li_2S_2 , and Li_2S versus discharge capacity, based on our model, Equations 17–21.

The results presented in Figures 8 and 9 represent the first step in quantifying the rates of reactions that occur in a sulfur cathode. Our simple discharge reaction models is also consistent with the reaction mechanism proposed by Hagen et al.²⁴ Most other studies suggest

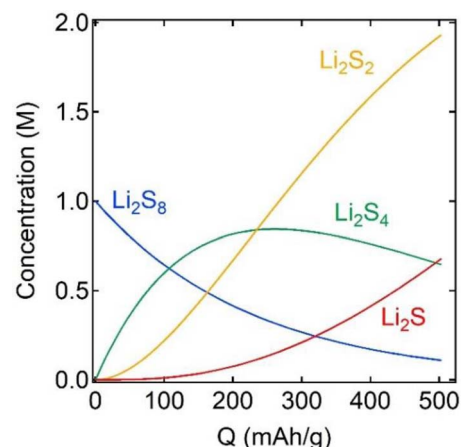
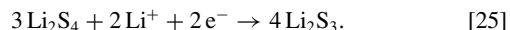


Figure 9. Concentration profile of Li_2S_8 , Li_2S_4 , Li_2S_2 , and Li_2S predicted by model.

that the reduction of sulfur in the cathode during discharge is likely to follow more complex schemes. For example, Barchasz et al.²¹ have proposed the following reaction for the reduction of Li₂S₄:



Such reactions require concerted action on several reactant molecules. In the example above, three Li₂S₄ molecules must react with two Li⁺ and two e⁻ to yield the stated product. In contrast, the proposed reaction for Li₂S₄ (Equation 5) only involves one reactant molecule. The additional complication with Equation 25 is the fact that the reaction must involve many steps wherein the Li₂S₄ molecules are cleaved and then recombine to give four Li₂S₃ molecules. For these reasons, Equation 5 is more likely to proceed than Equation 25.

The reaction rates that we present are only applicable to the regime $0 \leq Q \leq 500$ mAh/g (the discharge range covered by our experiments). It is likely that these rates will change as Li₂S becomes the dominant species in the cathode. The shorter-chain polysulfides such as Li₂S₂ are insoluble^{46–48} and thus their concentration near reaction sites in the cathode may be significantly different from the bulk concentration. In addition to electrochemical reactions, polysulfides can interconvert through chemical reactions. Sophisticated models that include transport are needed to account for complications arising from polysulfide dissolution and concomitant shuttling effects. Further work is needed to explore the effects.

The subject of reaction mechanisms in sulfur cathode is of considerable current interest.^{21,27,51–57,28,31,32,35,38,42,49,50} Our detection of Li₂S at the very early stage of discharge (as seen in Figure 8c) is consistent with the findings of Waluś et al.,^{20,58} Cuisinier et al.,³³ and Conder et al.⁵² Similarly, the formation and subsequent consumption of Li₂S₄ up to 500 mAh/g of discharge in Figure 9 is similar to the findings of Dominko et al.,³⁶ Zhang et al.⁵⁵ and Zheng et al.⁵¹ Our results in Figure 9 also indicated a significant amount of Li₂S₂ inside the cathode at a depth of discharge of 500 mAh/g, which is consistent with the results of Kawase et al.⁵⁴ Reaction mechanisms in the sulfur cathode have also been studied using computational simulations by Burgos et al.⁵⁹ They found that a variety of radical and dianion species were formed in their simulation cell. However, S₈²⁻ dianions were formed at the early stage of discharge, S₄²⁻ dianions dominated the intermediate stage of discharge, and S₄²⁻ dianions dominated the late stage of discharge at low applied current density. Our experimental findings and approach are consistent with these results.

Conclusions

In this work, we presented an operando XAS study of a solid-state Li-S cell. The use of a block copolymer electrolyte enabled the construction of an all solid-state Li-S cell that could readily be probed by XAS. Li₂S₈ was used as the active material inside the cathode instead of S₈ to facilitate dispersion of the sulfur-containing species in the electrode. The main objective of the operando XAS experiment was to study the discharge process. By using a thin cathode with relatively low sulfur content, we demonstrated that the XAS signal reflected all of the sulfur-containing species located throughout the depth of the cell. The average chain-length of sulfur-containing species, $x_{\text{avg,cell}}$, was determined from the ratio of the areas under the main-edge and pre-edge XAS peaks located at 2473 and 2471 eV. The measured values of $x_{\text{avg,cell}}$ at a given depth of discharge was in excellent agreement with predictions based on the number of electrons delivered to the cell as measured by the potentiostat. In addition, the production of Li₂S as a function of depth of discharge was monitored by tracking the area under a unique XAS peak located at 2476 eV. The XAS measurements were used to estimate rate constants of discharge reactions presented in the introduction (Equations 4–6 where we introduced rate constants k_1 , k_2 and k_3). While the overall rate of reaction in the cathode is controlled by the current density used to discharge the cell, the relative rate constants, k_2/k_1 and k_3/k_1 , depend on the electronic structures of the polysulfides participating in the reactions. To our knowledge, this work presents the first estimate of relative rate constants for discharge reactions in Li-S cells.

It is well established that the rate at which Li-S cells can be charged and discharged is compromised by dissolution of polysulfides and the insulating nature of the reactants and products. In addition to these factors, the relative reaction rates may present fundamental limitations on the practical power density of Li-S batteries. The present study is only a step toward understanding these limitations.

Acknowledgments

This work was supported by the Assistant Secretary for Energy Efficiency and Renewable Energy, Office of Vehicle Technologies of the US Department of Energy under Contract DE-AC02-05CH11231 under the Battery Materials Research program. Use of the Stanford Synchrotron Radiation Lightsource, SLAC National Accelerator Laboratory, is supported by the U. S. Department of Energy, Office of Science, Office of Basic Energy Sciences under Contract No. DEAC02-76SF00515. We thank Mike Toney for helpful discussions, and for helping us get access to the XAS instrument at SLAC. The Advanced Light Source is supported by the Director, Office of Science, Office of Basic Energy Sciences, of the U. S. Department of Energy under Contract No. DE-AC02-05CH11231.

ORCID

Deep B. Shah  <https://orcid.org/0000-0001-7816-031X>
Nitash P. Balsara  <https://orcid.org/0000-0002-0106-5565>

References

- P. G. Bruce, S. A. Freunberger, L. J. Hardwick, and J.-M. Tarascon, "Li-O₂ and Li-S batteries with high energy storage," *Nat. Mater.*, **11**, 172 (2011).
- X. Ji and L. F. Nazar, "Advances in Li-S batteries," *J. Mater. Chem.*, **20**, 9821 (2010).
- A. Manthiram, Y. Fu, and Y. S. Su, "Challenges and prospects of lithium-sulfur batteries," *Acc. Chem. Res.*, **46**, 1125 (2013).
- P. T. Dirlam, R. S. Glass, K. Char, and J. P. Pyun, "The use of polymers in Li-S batteries: A review," *J. Polym. Sci. Part A Polym. Chem.*, **55**, 1635 (2017).
- A. Manthiram, Y. Fu, S. Chung, C. Zu, and Y. Su, "Rechargeable Lithium – Sulfur Batteries," *Chem. Rev.*, **114**, 11751 (2014).
- Y. X. Yin, S. Xin, Y. G. Guo, and L. J. Wan, "Lithium-sulfur batteries: Electrochemistry, materials, and prospects," *Angew. Chemie - Int. Ed.*, **52**, 13186 (2013).
- Y. V. Mikhaylik and J. R. Akridge, "Polysulfide Shuttle Study in the Li/S Battery System," *J. Electrochem. Soc.*, **151**, A1969 (2004).
- M. Wild et al., "Lithium sulfur batteries, a mechanistic review," *Energy Environ. Sci.*, **8**, 3477 (2015).
- E. Zhao et al., "Advanced Characterization Techniques in Promoting Mechanism Understanding for Lithium-Sulfur Batteries," *Adv. Funct. Mater.*, **1707543**, 1 (2018).
- T. A. Pascal et al., "Liquid Sulfur Impregnation of Microporous Carbon Accelerated by Nanoscale Interfacial Effects," *Nano Lett.*, **17**, 2517 (2017).
- D. Zheng et al., "The Progress of Li – S Batteries — Understanding of the Sulfur Redox Mechanism:" *Dissolved Polysulfide Ions in the Electrolytes*, **1700233**, (2018).
- R. D. Rauh, K. M. Abraham, G. F. Pearson, J. K. Surprenant, and S. B. Brummer, "A Lithium/Dissolved Sulfur Battery with an Organic Electrolyte," *J. Electrochem. Soc.*, **126**, 523 (1979).
- H. Yamin, "Lithium Sulfur Battery," *J. Electrochem. Soc.*, **135**, 1045 (1988).
- S.-E. Cheon et al., "Rechargeable Lithium Sulfur Battery I," *J. Electrochem. Soc.*, **150**, A800 (2003).
- D. R. Wang, K. H. Wujcik, A. A. Teran, and N. P. Balsara, "Conductivity of Block Copolymer Electrolytes Containing Lithium Polysulfides," *Macromolecules*, **48**, 4863 (2015).
- D.-H. Han et al., "Time-Resolved In Situ Spectroelectrochemical Study on Reduction of Sulfur in N,N[^{sup}]'-Dimethylformamide," *J. Electrochem. Soc.*, **151**, E283 (2004).
- Y. Jung et al., "Effect of Organic Solvents and Electrode Materials on Electrochemical Reduction of Sulfur," *Int. J. Electrochem. Sci.*, **3**, 566 (2008).
- Y. C. Lu, Q. He, and H. A. Gasteiger, "Probing the lithium-sulfur redox reactions: A rotating-ring disk electrode study," *J. Phys. Chem. C*, **118**, 5733 (2014).
- J. Nelson et al., "In operando X-ray Diffraction and Transmission X-ray Microscopy of Lithium Sulfur Batteries," *J. Am. Chem. Soc.*, **134**, 6337 (2012).
- S. Waluś et al., "New insight into the working mechanism of lithium-sulfur batteries: in situ and operando X-ray diffraction characterization," *Chem. Commun. (Camb.)*, **49**, 7899 (2013).
- C. Barchasz, F. Molton, and C. Duboc, "Lithium/Sulfur Cell Discharge Mechanism: An Original Approach for Intermediate Species Identification," *Anal. Chem.*, **84**, 3973 (2012).
- N. A. Cañas, D. N. Fronczek, N. Wagner, A. Latz, and K. A. Friedrich, "Experimental and Theoretical Analysis of Products and Reaction Intermediates of Lithium–Sulfur Batteries," *J. Phys. Chem. C*, **118**, 12106 (2014).

23. K. H. Wujcik et al., "Lithium Polysulfide Radical Anions in Ether-Based Solvents," *J. Phys. Chem. C*, **120**, 18403 (2016).
24. M. Hagen et al., "In-Situ Raman Investigation of Polysulfide Formation in Li-S Cells," *J. Electrochem. Soc.*, **160**, A1205 (2013).
25. H. L. Wu, L. A. Huff, and A. A. Gewirth, "In situ raman spectroscopy of sulfur speciation in lithium-sulfur batteries," *ACS Appl. Mater. Interfaces*, **7**, 1709 (2015).
26. L. A. Huff, J. L. Rapp, J. A. Baughman, P. L. Rinaldi, and A. A. Gewirth, "Identification of lithium-sulfur battery discharge products through 6Li and 33S solid-state MAS and 7Li solution NMR spectroscopy," *Surface Science*, **631**, 295 (2015).
27. K. A. See et al., "Ab initio structure search and in situ 7Li NMR studies of discharge products in the Li-S battery system," *J. Am. Chem. Soc.*, **136**, 16368 (2014).
28. J. Gao, M. A. Lowe, Y. Kiya, and H. D. Abruña, "Effects of liquid electrolytes on the charge-discharge performance of rechargeable lithium/sulfur batteries: Electrochemical and in-situ X-ray absorption spectroscopic studies," *J. Phys. Chem. C*, **115**, 25132 (2011).
29. M. A. Lowe, J. Gao, and H. D. Abruña, "Mechanistic insights into operational lithium-sulfur batteries by in situ X-ray diffraction and absorption spectroscopy," *RSC Adv.*, **4**, 18347 (2014).
30. L. Zhang, D. Sun, J. Feng, E. J. Cairns, and J. Guo, "Revealing the electrochemical charging mechanism of nano-sized Li₂S by in-situ and operando X-ray absorption spectroscopy," *Nano Lett.*, **17**, 5084 (2017).
31. E. C. Miller, R. M. Kasse, K. N. Heath, B. R. Perdue, and M. F. Toney, "Operando Spectromicroscopy of Sulfur Species in Lithium-Sulfur Batteries," *J. Electrochem. Soc.*, **165**, A6043 (2018).
32. M. Cuisinier et al., "Sulfur Speciation in Li - S Batteries Determined by Operando X - ray Absorption Spectroscopy," *J. Phys. Chemistry Lett.*, **4**, 3227 (2013).
33. M. Cuisinier et al., "Unique behaviour of nonsolvents for polysulphides in lithium-sulfur batteries," *Energy Environ. Sci.*, **7**, 2697 (2014).
34. M. Cuisinier, C. Hart, M. Balasubramanian, A. Garsuch, and L. F. Nazar, "Radical or Not Radical: Revisiting Lithium-Sulfur Electrochemistry in Nonaqueous Electrolytes," *Adv. Energy Mater.*, **5**, 1 (2015).
35. M. U. M. Patel and R. Dominko, "Application of in operando UV/Vis spectroscopy in lithium-sulfur batteries," *ChemSusChem*, **7**, 2167 (2014).
36. R. Dominko et al., "Analytical Detection of Polysulfides in the Presence of Adsorption Additives by Operando X-ray Absorption Spectroscopy," *J. Phys. Chem. C*, **119**, 19001 (2015).
37. K. H. Wujcik et al., "Characterization of Polysulfide Radicals Present in an Ether-Based Electrolyte of a Lithium-Sulfur Battery during Initial Discharge Using in Situ X-Ray Absorption Spectroscopy Experiments and First-Principles Calculations," *Adv. Energy Mater.*, **5**, (2015).
38. Y. Gorlin et al., "Operando Characterization of Intermediates Produced in a Lithium-Sulfur Battery," *J. Electrochem. Soc.*, **162**, A1146 (2015).
39. Y. Gorlin et al., "Understanding the Charging Mechanism of Lithium-Sulfur Batteries Using Spatially Resolved Operando X-Ray Absorption Spectroscopy," *J. Electrochem. Soc.*, **163**, A930 (2016).
40. N. Hadjichristidis, H. Iatrou, S. Pispas, and M. Pitsikalis, "Anionic polymerization: high vacuum techniques," *J. Polym. Sci. Part A Polym. Chem.*, **38**, 3211 (2000).
41. U. C. Berkeley and A. Andrew, Block Copolymer Electrolytes: Thermodynamics, Ion Transport, and Use in Solid- State Lithium / Sulfur Cells By Alexander Andrew Teran A dissertation submitted in partial satisfaction of the requirements for the degree of Doctor of Philosophy in Chemica. (2013).
42. K. H. Wujcik, D. R. Wang, T. A. Pascal, D. Prendergast, and N. P. Balsara, "In Situ X-ray Absorption Spectroscopy Studies of Discharge Reactions in a Thick Cathode of a Lithium Sulfur Battery," *J. Electrochem. Soc.*, **164**, A18 (2017).
43. D. T. Hallinan Jr. and N. P. Balsara, "Polymer Electrolytes," *Annu. Rev. Mater. Res.*, **43**, 503 (2013).
44. T. A. Pascal et al. *The X-ray Absorption Spectra of Dissolved Polysulfides in Lithium - Sulfur Batteries from First Principles.*, (2014).
45. Q. Wang et al., "Direct Observation of Sulfur Radicals as Reaction Media in Lithium Sulfur Batteries," *J. Electrochem. Soc.*, **162**, A474 (2015).
46. G. Yang, S. Shi, J. Yang, and Y. Ma, "Insight into the role of Li₂S₂ in Li-S batteries: a first-principles study," *J. Mater. Chem. A*, **3**, 8865 (2015).
47. A. Paoletta et al. Transient existence of crystalline lithium disulfide Li₂S₂ in a lithium-sulfur battery. *J. Power Sources*, **325**, 641 (2016).
48. Z. Liu, P. B. Balbuena, and P. P. Mukherjee, "Revealing Charge Transport Mechanisms in Li₂S₂ for Li-Sulfur Batteries," *J. Phys. Chem. Lett.*, **8**, 1324 (2017).
49. M. Minelli, M. Giacinti Baschetti, D. T. Hallinan, and N. P. Balsara, "Study of gas permeabilities through polystyrene-block-poly(ethylene oxide) copolymers," *J. Memb. Sci.*, **432**, 83 (2013).
50. C. W. Lee et al., "Directing the Lithium-Sulfur Reaction Pathway via Sparingly Solvating Electrolytes for High Energy Density Batteries," *ACS Cent. Sci.*, **3**, 605 (2017).
51. D. Zheng et al., "Investigation of the Li-S Battery Mechanism by Real-Time Monitoring of the Changes of Sulfur and Polysulfide Species during the Discharge and Charge," *ACS Appl. Mater. Interfaces*, **9**, 4326 (2017).
52. J. Conder et al., "Direct observation of lithium polysulfides in lithium-sulfur batteries using operando X-ray diffraction," *Nat. Energy*, **2**, 1 (2017).
53. W. Zhu et al., "Investigation of the reaction mechanism of lithium sulfur batteries in different electrolyte systems by in situ Raman spectroscopy and in situ X-ray diffraction," *Sustain. Energy Fuels*, **1**, 737 (2017).
54. A. Kawase, S. Shirai, Y. Yamoto, R. Arakawa, and T. Takata, "Electrochemical reactions of lithium-sulfur batteries: An analytical study using the organic conversion technique," *Phys. Chem. Chem. Phys.*, **16**, 9344 (2014).
55. L. Zhang, D. Sun, J. Feng, E. J. Cairns, and J. Guo, "Revealing the electrochemical charging mechanism of nanosized Li₂S by in situ and operando X-ray absorption spectroscopy," *Nano Lett.*, **17**, 5084 (2017).
56. N. A. Cañas, S. Wolf, N. Wagner, and K. A. Friedrich, "In-situ X-ray diffraction studies of lithium-sulfur batteries," *J. Power Sources*, **226**, 313 (2013).
57. M. U. M. Patel et al., "X-ray Absorption Near-Edge Structure and Nuclear Magnetic Resonance Study of the Lithium-Sulfur Battery and its Components," *ChemPhysChem*, **15**, 894 (2014).
58. S. Waltš et al., "Lithium/Sulfur Batteries Upon Cycling: Structural Modifications and Species Quantification by in Situ and Operando X-Ray Diffraction Spectroscopy," *Adv. Energy Mater.*, **5**, 1 (2015).
59. J. C. Burgos, P. B. Balbuena, and J. A. Montoya, "Structural Dependence of the Sulfur Reduction Mechanism in Carbon-Based Cathodes for Lithium - Sulfur Batteries," *J. Phys. Chem. C*, **121**, 18369 (2017).